

Detecting Winds Aloft from Water Vapour Satellite Imagery in the Vicinity of Storms

by

Robert M. Rabin^{1,3}, Stephen F. Corfidi², Jason C. Brunner³, Carl E. Hane¹

NOAA/National Severe Storms Laboratory (NSSL), Norman, OK¹

NOAA/Storm Prediction Center (SPC), Norman, OK²

Cooperative Institute for Meteorological Satellite Studies (CIMSS), Madison, WI³

January 2004

Revised for

Weather

Author's address for correspondence:

Dr. Robert M. Rabin
NOAA/National Severe Storms Laboratory
1313 Halley Circle
Norman, OK 73069 USA

Introduction

The most extensive use of water vapour imagery in recent years has been to identify upper-level wind features such as short-wave troughs and to compare their location and intensity to those produced by numerical forecast models. For example, Weldon and Holmes (1991) compiled a catalogue of water vapour imagery for use in identifying a wide range of upper air features. The identification of these features arises from spatial patterns of brightness in the water vapour images (related to the variation of radiance with moisture content in the upper troposphere). Subjective adjustments to forecasts can be made from observed differences in the location and intensity of troughs, jets, and other features in satellite imagery to those in model analyses and forecasts.

In addition to the subjective use of water vapour imagery in forecasting, the imagery has been used quantitatively to provide estimates of the wind through movement of clouds and moisture features between successive images, where direct measures from weather balloons are lacking. Winds were determined by manually tracking clouds between successive images and calculating the wind from the displacement and the time interval between images, in the early years of this type of research (Stewart et al., 1985). The height of the wind estimate was derived from the cloud top temperature and a vertical profile of temperature. This presupposes that the cloud moves with the speed of the wind, an assumption that is not strictly valid. Comparisons with independent balloon measurements suggest an underestimation of wind speed and the need for an empirical adjustment. In recent years, the technique has been automated and is based on cross correlation of the patterns within boxes which are displaced according to the winds from a forecast model 'guess' field (Velden et al., 1997). With this approach, winds cannot only be estimated from tracking clouds, but also from the displacement of small-scale structures present in clear areas of the imagery. These structures occur due to

humidity fluctuations in the middle and upper layers of the troposphere.

While winds obtained from tracking cloud features in the imagery are prone to greater uncertainty than balloon measurements, they have been used to improve analyses and forecasts over ocean areas (Goerss et al., 1998; Langland et al., 1999; Soden et al., 2001; Xiao et al., 2002). In order to explore the use of satellite winds over land, an automated method for calculating water vapour winds, developed at the Cooperative Institute for Meteorological Satellite Studies, CIMSS (Velden et al., 1997), is being applied to geostationary satellite imagery on an experimental basis in the U.S. Derived wind fields are being made available on an experimental basis, to the U.S. National Oceanic and Atmospheric Administration's (NOAA) Storm Prediction Center (SPC). The editing of wind vectors is kept at a minimum in order to include significant deviations from the model 'guess' field. This allows the detection of perturbed flow aloft due to thunderstorms and other small-scale features that are not correctly captured by forecast models. A new set of winds is computed every 30 minutes from Geostationary Operational Environmental Satellite (GOES-12) imagery. With the new capabilities of the Meteosat Second Generation (MSG) satellite (Schmetz et al., 2002), generation of winds over Europe will be possible with the same or greater frequency and spatial resolution as described here.

The main purpose of this article is to demonstrate how the satellite-derived winds can be used to capture features on a more detailed scale than from conventional meteorological observations. Examples of the upper-level wind fields deduced from water vapour imagery are illustrated for summertime thunderstorm events. The winds are used to track upper air features such as jet maxima, and divergent regions where vertical air motion and convective development might be enhanced.

Method

The automated technique relies on a forecast wind field to facilitate the location of common features between successive images. The forecast winds used are from the U.S. Navy Operational Global Atmospheric Prediction System (NOGAPS) model (Rosmond, 1992). By employing a model with relatively low spatial resolution such as the NOGAPS, the addition of higher resolution winds from the satellite is more clearly identifiable. Current implementation utilizes time interpolation to provide hourly updates of the background wind field between forecast output times. It is important to note that the winds from features tracked in water vapour imagery (other than clouds) are not associated with a single altitude. Rather, these winds are representative of layers, weighted in the vertical in accordance with the weighting function of the GOES Imager water vapour channel, centred at 6.7 microns. (Covering Europe, the MSG has two water vapour bands centred on 6.2 and 7.3 microns). For clear skies, most of the weight typically comes from a layer on the order of 200 hPa thick, or about 20% of the total depth of the troposphere. (Velden et al., 1997, Fig. 3, gives a typical weighting function). The precise thickness of this layer depends on the uniformity of the vertical moisture profile, and it can be thinner where pronounced peaks in moisture occur in the vertical (Rao et al., 2002). The height of the layer within the troposphere varies directly with upper-level moisture. Typically, for clear sky conditions, the mean pressure level of the layer varies from near 300 hPa when upper-level moisture is high, to 500 hPa or at lower altitudes when the atmosphere is dry and cold. Wind vectors directly associated with thick high clouds, such as anvil tops, are derived from a much thinner layer than those obtained in clear sky conditions. In these cases, the mean pressure level is typically at 200 hPa or higher altitudes.

Comparisons of satellite-derived winds with rawinsondes (balloons) suggest root-mean square errors (RMSE) of roughly 7 m s^{-1} (Velden et al., 1997). However, total uncertainty may

be significantly less given the sampling differences between rawinsondes and satellite winds and that rawinsonde errors themselves average 3 m s^{-1} .

Since the mean height of wind vectors varies over a given region, it is necessary to interpolate the values to a constant altitude before evaluation of horizontal gradients required in the computation of kinematic parameters such as vorticity and divergence. For this purpose, an objective analysis is used which combines available wind vectors with the guess wind field at constant pressure levels from the NOGAPS forecast model. Grid spacing of about 100 km has been used for this analysis. Analyses centred near 300 hPa are generally used for evaluation of divergence (in a horizontal plane), vorticity (rotation about a vertical axis), and wind speed. Because of the vertical weighting of the water vapour winds, the derived quantities such as divergence and vorticity represent vertical averages centred near 300 hPa. This layer often encompasses the typical anvil height of thunderstorms, where upper-level divergence can be strong as a result of vigorous upward air motion below. Caution should be exercised in interpreting the kinematic properties near dry areas where no satellite winds may be available near 300 hPa. The objectively analysed winds are based mainly on the guess wind field in such areas. A map of satellite-derived wind vectors can be examined to ensure adequate coverage in the 200-400 hPa layer, and, if necessary, the analysis level can be varied depending on the mean height of the wind vectors.

Displays of the wind properties are available on the web for real time data and for archived cases¹. (Current location of the web page can be obtained from the authors). The web page includes interactive displays of water vapour imagery animation and overlays of derived parameters. Comparisons are also available between the analysed fields of divergence, vorticity, and wind speed and the same fields from the NOGAPS forecasts and hourly analyses from a higher resolution forecast model, the Rapid Update Cycle (RUC-2) (Benjamin et al.,

¹ At time of writing: http://cimss.wisc.edu/mesoscale_winds

1998). In its current implementation, the RUC-2 model uses hourly observations including satellite cloud and humidity data, but no satellite winds over land.

Long Duration Convective Systems

The lifetimes of thunderstorms range from less than an hour for small, individual cells to many hours for large clusters. Large storm clusters, known as Mesoscale Convective Systems (MCSs), often develop under weak upper forcing during the summer in the U.S., Europe, and other mid-latitude regions. Energised by moisture and warm air advection in the low levels, they typically occur in the vicinity of upper level ridges. Although the general environmental conditions for these systems are known, they remain difficult to forecast. The presence of a moist layer and upward air motion through at least the lower part of the troposphere can lead to destabilization and the formation of convective storms. Once storms form, the upward motion intensifies in local updrafts through the entire troposphere. These updrafts decelerate as they become negatively buoyant in the upper troposphere or lower stratosphere. The air is forced to diverge horizontally and is accompanied by the characteristic anvil clouds at the top of thunderstorms. Blanchard et al. (1998) proposed a key role of inertial instability, when sufficient anti-cyclonic wind shear on the equatorward side of jet streams occurs, in the growth of MCSs. This condition can enhance upper level divergence and sustained upward air motion. Using upper wind analyses from balloon data, they found that the occurrence of negative absolute vorticity, a necessary condition for inertial instability, accompanied the onset of large systems. The satellite wind analyses provide an excellent opportunity to examine the absolute vorticity in detail along with the development of divergence aloft.

The time series of maximum divergence is shown in Figure 1 for a large MCS that existed for 14 hours on 20 July 1995. This system developed along a front and took on the

elongated shape typical of a squall line MCS. The surface front preceded an upper tropospheric trough. Over most of the lifetime of the system, the maximum divergence was inversely proportional to the mean cloud shield temperature observed in the infrared satellite imagery (Figure 1a). The strongest divergence (0430 UTC) is associated with the most intense updrafts and thus the coldest cloud top temperatures (indicative of the highest cloud top height). The period of sustained, rapid increase in divergence (0100-0430 UTC) matches the time when the cold cloud shield above the MCS was expanding most rapidly, as evidenced by the time series of cloud top area shown in Figure 1b. As the magnitude of divergence abruptly decreased (0430-0700 UTC), the expansion began to slow. After some lag in time, the size of the cloud shield became constant (Figure 1b, 0630-0830 UTC) and then steadily diminished the size. Unlike during the growth stage, the rate of decay of the cloud shield is not well related to the divergence. Other factors such as entrainment of dry air and sublimation were likely important.

During the early stages of development (2300-0300 UTC), the minimum absolute vorticity was just south of the convection located in southeast Nebraska (Fig. 2a). The system moved to the south, in the direction of the minimum vorticity, as it grew in coverage and intensity. During the mature phase, the minimum absolute vorticity was aligned roughly with the convection (Fig. 2b); however, the minimum was located downwind (northeast) of the most active area. In this downwind area, the absolute vorticity became negative. During the decay phase, the minimum remained aligned with the convective cloud, but was slightly positive (not shown). Although reformation along propagating surface outflow boundaries (e.g., Corfidi, 2003) was likely the principal cause of growth of the MCS toward the south, inertial instability may have also been an important factor leading to preferred growth to the south during the early stages of development. Following the theory proposed by Blanchard et al. (1998), divergent flow (normal to the prevailing flow) would be enhanced where the absolute vorticity became negative (in this case to the south of the active thunderstorms).

Detecting Subtle Disturbances in Weak Upper Flow

While distinct upper troughs can be identified easily from the weather balloon network over land, weak disturbances are more difficult to detect. Weak disturbances can be a factor in thunderstorm formation when fronts or other convergence lines are not present to provide a focus for upward air motion. This is especially true when a small amount of inhibition is present to restrict deep convective overturning in the atmosphere. Shaw (1942) termed this inhibition a "valve", caused by an inversion in the temperature profile above the surface. (Today meteorologists refer to this structure as a "capping inversion", and refer to the amount of energy required for air parcels to overcome negative buoyancy below the lid as "convective inhibition"). The following examples are based on the experiences of one of the authors (SC) in forecasting thunderstorm development on a national scale at the Storm Prediction Center. They illustrate rapid evolution in upper level divergence as diagnosed from the satellite wind analyses during the late afternoon in areas where the "capping" inversion had weakened due to solar heating of the earth's surface. In each case, strong convergence was absent at the surface and the forecast of thunderstorm development was especially difficult. The analyses shown are all at 300 hPa, unless otherwise noted.

02 June 2003

On 2 June, the upper flow was from the west-northwest over Colorado, with a wind speed maximum to the east in Kansas. The distribution of wind observations from weather balloons and satellite on this day can be compared in Fig. 3. From the satellite-derived winds, a distinct band of divergent air is centred over Colorado at 2145 UTC (Fig. 4b). The divergence appears where the air accelerates eastward into the speed maximum (Fig. 3b). Given the

relatively coarse distribution of the balloon wind observations, the speed maximum cannot be resolved in Fig. 3a. The divergence over Colorado was absent at 1745 UTC (Fig. 4a), indicating development during the four hours preceding 2145 UTC. Note that the forecast, used as a first guess for the satellite winds analysis, is void of the same divergence pattern (Fig. 5a). In general, the patterns in the first guess lack the detail of the satellite analysis. This is to be expected because of the relatively coarse grid used by the global forecast model (NOGAPS). In contrast, the mesoscale model analysis (RUC-2) includes more detail than the satellite analysis (Fig. 5b). Despite the differences in detail, the divergence in Colorado appears in both the mesoscale model and satellite analysis. By 0045 and 0345 UTC 03 June 2003 (Fig. 4c-d), thunderstorms had developed in this area of divergence as it moved to the southeast. At these times the divergence patterns were less linear and more circular in shape. Balloon observations near these areas indicated that a capping inversion was present in the late afternoon. It appears that upward air motion associated with the divergence aloft provided a favourable condition for storm initiation during the afternoon.

11-12 June 2003

During this two-day period, the main belt of westerly winds extended across the northern tier of states, while a weaker southern jet stream extended from Arizona to New Mexico to the lower Mississippi Valley. The vertical wind shear and thermodynamic environment were supportive of organized severe convection in the vicinity of the southern jet, especially in western Texas, provided that sufficient lifting could be realized to overcome a persistent capping inversion. A wind shift, depicted across the nearly stationary dryline in Figs. 6a and 9, provided some convergence and a source for the lifting of surface air.

Thunderstorms developed over west Texas by 0000 UTC 12 June (Fig. 7b). Although low-level forcing mechanisms were lacking (surface convergence was weak in the vicinity of the

dryline over the region, Fig. 6a), the storms quickly became severe, producing large hail, damaging winds and a few tornadoes as they spread eastward toward the central part of Texas (Fig 6b). The storms formed near the dryline along the western edge of a region of sustained divergence, based on satellite-derived winds. The divergence was present 4-5 hours prior to thunderstorm development (Fig. 7a). It is expected that the upward air motion associated with this divergence contributed to weakening of the capping inversion and deepening the moist boundary layer in a localised region near the dryline. This divergence was not apparent in the first guess wind field, shown in Fig. 8.

In contrast to the previous day's activity, thunderstorms failed to develop over west Texas on 12 June 2003, despite the presence of similar thermodynamic conditions and low-level forcing mechanisms (Fig. 9). In this case, the mid- and upper-level flow was even more zonal (straight west-east) than on the preceding day, making identification and tracking of waves in the southern jet particularly difficult. The satellite-derived fields, however, included a region of sustained upper-level convergence over west Texas on the afternoon and evening of 12 June (Fig. 10a). It should be noted that the forecast, used as a first guess for the satellite winds analysis, indicated convergence of less magnitude over the same region (Fig. 10b). The downward air motion associated with the convergence appeared to be at least partly responsible for the absence of convective initiation across the region (Doswell et al., 2002). The satellite data provided increased confidence that the threat for severe weather would remain low even though standard diagnostic and forecast tools (such as objective fields of surface-based instability and convergence) suggested otherwise.

Concluding Remarks

The assimilation of satellite-derived winds into numerical forecast models requires a

relatively close matching of the satellite observations to the presumed winds from model fields. Observations that deviate significantly from the model winds must be discarded in order to prevent adverse effects in the forecasts. This raises a philosophical dilemma as to how to utilise (or ignore) data much different than expected from other analyses. As models are run at higher resolution, it seems more feasible to include such features as the disturbed airflow near MCSs. The inclusion of accurate upper-level divergence and vorticity and their changes over short time intervals should be important both for forecasting the near-term and long-term evolution of the system, in addition to forecasting any perturbations that remain after the complete dissipation of the MCS.

In the applications of satellite wind observations reviewed in this paper, deviations from the large-scale wind field are emphasized in order to examine the effects of convection and other mesoscale features. The horizontal resolution of wind fields is limited by the number of features in the water vapour imagery tracked by the automated technique, and by the resolution of the objective analysis. For example, the fields of divergence and vorticity do not contain as much detail as the RUC-2 model. Nevertheless, the satellite analyses are useful in resolving upper-level divergence and vorticity fields with superior temporal and spatial resolution than is possible from most other observational sources. Divergence patterns are sometimes useful in diagnosing areas of vertical air motion prior to possible convective development, especially when synoptic forcing and surface fronts are lacking. In addition, the satellite-winds capture the divergence that develops as a consequence of storm updrafts and can be useful in diagnosing the extent and intensity of storm clusters. Other uses include tracking upper-level features, and comparing locations and intensity with forecast models.

The principal limitations of the water vapour wind analysis are the variable nature and uncertainty of the target heights and the lack of vertical profiling. The future implementation of the Geostationary Imaging Fourier Transform Spectrometer (GIFTS) by U.S. National

Aeronautics and Space Administration (NASA) has the potential to provide analysis of water vapour winds at multiple levels due to the improved vertical resolution provided by its hyperspectral observations (Smith et al., 2001; 2002).

Acknowledgments

We wish to thank Steve Wanzong, Tim Olander, David Stettner, and Chris Velden, of the CIMSS for their encouragement and assistance in setting up the software for satellite winds processing. Also, the concept of satellite winds would not have been possible without the foresight of Dr. Vern Suomi and early developers at the University of Wisconsin Space Science and Engineering Center (SSEC) from the 1970's onward. The Man computer Interactive Data Access System (McIDAS) developed at SSEC was used for the generation of displays and objective analyses (Lazzara et al., 1999). Thanks to Tom Whittaker, also of SSEC, for developing the Java Applets used for the dynamic presentation of output on the real-time web site. A portion of the work was supported by COMET grant SOO-18114 through a NWS cooperative project.

References

- Benjamin, S.G., J.M. Brown, K.J. Brundage, G.J. DiMego, L.L. Morone, B. Schwartz, T. Smirnova, and T.L. Smith, 1998: The operational RUC-2. Preprints, 16th Conference on Weather Analysis and Forecasting, AMS, Phoenix, 249-252.
- Blanchard, D.O., W.R. Cotton, and J.M. Brown, 1998: Mesoscale circulation growth under conditions of weak inertial instability. *Mon. Wea. Rev.*, **126**, 118-140.
- Corfidi, S.F., 2003: Cold pools and MCS propagation: Forecasting the motion of downwind developing MCSs. *Weather and Forecasting*, **18**, 997-1017.
- Doswell, C.A., C. A., Baker, D. V., Liles, C. A. 2002: Recognition of negative mesoscale factors for severe-weather potential: A case study. *Weather and Forecasting*, **17**, 937-954.
- Goerss, J., C.S. Velden, J. Hawkins, 1998: The impact of multispectral GOES-8 wind information on Atlantic tropical cyclone track forecasts in 1995. Part 2: NOGAPS forecasts. *Mon. Wea. Rev.*, **126**, 1219-1227.
- Langland, R.H., Z. Toth, R. Gelaro, I. Szunyogh, M.A. Shapiro, S.J. Majumdar, R.E. Morss, G.D. Rohaly, C. Velden, N. Bond, C.H. Bishop, 1999: The North Pacific Experiment (NORPEX-98): Targeted observations for improved North American Weather Forecasts. *Bull. Amer. Meteor. Soc.*, **80**, 1363-1384.

Lazzara, M.A., J.M. Benson, R.J. Fox, D.J. Laitsch, J.P. Rueden, D.A. Santek, D.M. Wade, T.M. Whittaker, and J.T. Young, (1999): The Man computer Interactive Data Access System: 25 Years of Interactive Processing. *Bull. Amer. Meteor. Soc.*, **80**, pp 271-284.

Rao, P.A., C.S. Velden, S.A. Braun, 2002: The vertical error characteristics of GOES-derived winds: Description and experiments with numerical weather prediction. *J. Appl. Meteor.*, **41**, 253-271.

Rosmond, T.E., 1992: The design and testing of the Navy Operational Global Atmospheric Prediction System. *Wea. Forecasting*, **7**, 262-272.

Schmetz, J., Pili, P., Tjemkes, S., Just, D., Kerkmann, J., Rota, S., Ratier, A.. 2002: An Introduction to Meteosat Second Generation (MSG). *Bulletin of the American Meteorological Society*: Vol. 83, No. 7, pp. 977-992.

Shaw, W. N., 1942: *Manual of Meteorology, Volume III, The Physical Processes of Weather*. Cambridge University Press.

Smith, W.L., F. Harrison, D. Hinton, J. Miller, M. Bythe, D. Zhou, H. Revercomb, F. Best, H. Huang, R. Knuteson, D. Tobin, C. Velden, G. Bingham, R. Huppi, A. Thurgood, L. Zollinger, R. Epslin, R. Peterson, 2001: The Geostationary Imaging Fourier Transform Spectrometer (GIFTS). 11th Conference on Satellite Meteorology and Oceanography, Madison, WI, 15-18 October 2001. Boston, Amer. Meteor. Soc., 700-707.

Smith, W.L., F.W. Harrison, D.E. Hinton, H.E. Revercomb, G.E. Bingham, R. Petersen, J.C.

Dodge, 2002: GIFTS-The precursor geostationary satellite component of the future earth observing system. International Geoscience and Remote Sensing Symposium, 2002.

Proceedings,v.1. Piscataway, NJ, IEEE, 357-361.

Soden, B.J., C.S. Velden, R.E. Tuleya, 2001: The impact of satellite winds on experimental GFDL hurricane model forecasts. *Mon. Wea. Rev.*, **129**, 835-852.

Stewart, T.R., C. M. Hayden, W.L. Smith, 1985: A note on water-vapor wind tracking using VAS on McIDAS. *Bull. Amer. Meteor. Soc.*, **66**, 1111-1115.

Velden, C.S., C.M. Hayden, S. Nieman, W.P. Menzel, S. Wanzong, and J. Goerss, 1997: Upper-tropospheric winds derived from geostationary satellite water vapor observations. *Bull. Amer. Meteor. Soc.*, **78**, 173-195.

Weldon, R.B., and S.J. Holmes, 1991: Water vapor imagery: Interpretation and applications to weather analysis and forecasting. NOAA Tech. Rep. NESDIS 67, 213 pp.

Xiao, Q., X. Zou, M. Ponca, M.A. Shapiro, C. Velden, 2002: Impact of GMS-5 and GOES-9 satellite derived winds on the prediction of a NORPEX extratropical cyclone. *Mon. Wea. Rev.*, **130**, 507-528.

Figure Captions

Figure 1. Time series of divergence (solid, 10^{-5}s^{-1}) for the 20 July 1995 MCS with superimposed times series of (a) mean cloud top temperature (dotted, $^{\circ}\text{K}$) and (b) area of cloud top colder than -55°C (dotted, 10^5 km^2). Diamonds indicate the times at which time averages (3-point means) in divergence were available.

Figure 2. GOES-8 water vapour imagery, divergence (yellow, 10^{-5}s^{-1}), absolute vorticity (red, 10^{-5}s^{-1}), and wind barbs (knots) at: a) 2300 UTC 19 July 1995, and b) 0445 UTC 20 July 1995.

Figure 3. Upper air winds at 0000 UTC on 03 June 2003 from (a) synoptic weather balloons, and (b) satellite. The states of Colorado (CO), Kansas (KS), and Arkansas (AR) are noted. The area outlined in green is that shown in Figures 4-5. In (a), wind barbs (knots) are from observations at 300 hPa. Streamlines (grey) and isotachs (blue): 50, 75, and 100 kt (25, 32, and 50 ms^{-1}) are included. In (b), isotachs (red, knots) are from objectively analysed winds at 300 hPa, wind barbs (knots) are from the satellite-based winds (the average pressure of these winds vary, black: 100-250, cyan: 251-350, yellow: 351-500 hPa). Water vapour imagery is in the background.

Figure 4. GOES-12 water vapour imagery and divergence at 300 hPa (10^{-5}s^{-1}) derived from satellite-winds on 02 June 2003 at a) 1745 UTC and b) 2145 UTC. Solid contours are positive (divergence) and dash contours are negative (convergence).

Figure 5. GOES-12 water vapour imagery and divergence at 300 hPa (10^{-5}s^{-1}) on 02 June

2003 at a) 2145 UTC from the first guess (NOGAPS model), and b) 1945 UTC from the RUC-2 mesoscale model analysis. Solid contours are positive (divergence) and dash contours are negative (convergence).

Figure 6. a) Surface weather map at 2300 UTC, 11 June 2003. Observations plotted are from the standard station model: wind flags (kts), temperature (upper left) and dew point (lower left) in degrees F, sea level pressure (upper right, last three digits of pressure in 10^{-1} hPa). Contours show sea level pressure (last two digits are labelled; for example, "04" indicates 1004 hPa). Fronts have solid barbs. Small barbs indicate outflow boundaries from rain-cooled air. Open barbs indicate a dryline (separating hot, dry air with a westerly wind component off the mountains from moist air with a southerly component from the Gulf of Mexico). Broken lines are dissipating fronts, b) Location of severe weather reports during the 24 hour period beginning at 1200 UTC on 11 June: wind damage (blue), large hail (green), and tornadoes (red).

Figure 7. GOES-12 water vapour imagery and divergence at 300 hPa (10^{-5}s^{-1}) derived from satellite-winds, a) 11 June 2003 at 1945 UTC, b) 12 June 2003 at 0045 UTC. Solid contours are positive (divergence) and dash contours are negative (convergence).

Figure 8. GOES-12 water vapour imagery and divergence at 300 hPa (10^{-5}s^{-1}) from first guess model (NOGAPS), a) 11 June 2003 at 1945 UTC, b) 12 June 2003 at 0045 UTC. Solid contours are positive (divergence) and dash contours are negative (convergence).

Figure 9. Surface weather map at 2300 UTC, 12 June 2003. Notations are the same as in Fig. 6a.

Figure 10. GOES-12 water vapour imagery and divergence at 300 hPa (10^{-5}s^{-1}) on 12 June 2003 at 2145 UTC, a) derived from satellite-winds, and b) from the first guess model (NOGAPS). Solid contours are positive (divergence) and dash contours are negative (convergence).

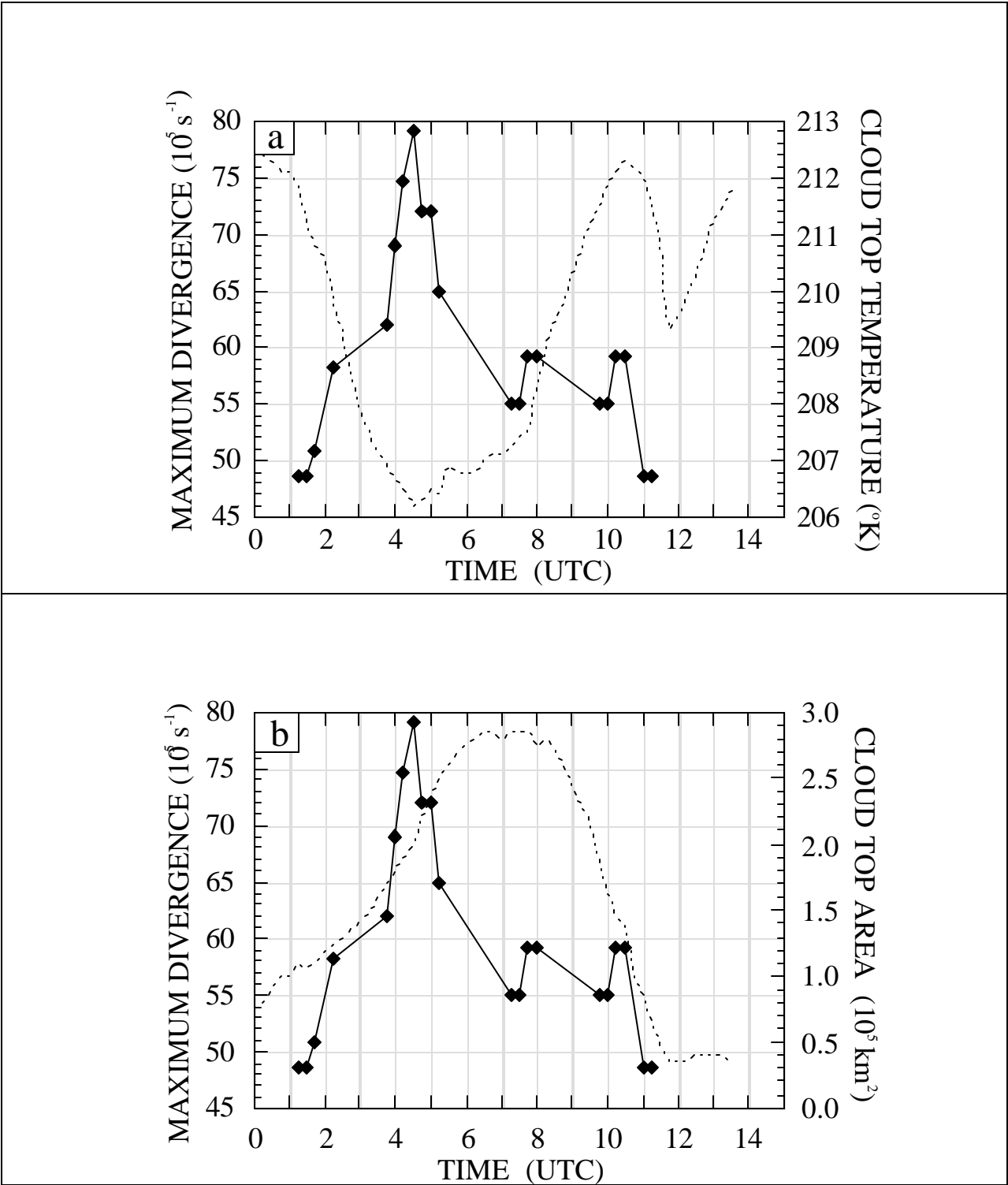


Figure 1. Time series of divergence (solid, 10^5 s^{-1}) for the 20 July 1995 MCS with superimposed times series of (a) mean cloud top temperature (dotted, $^{\circ}\text{K}$) and (b) area of cloud top colder than -55°C (dotted, 10^5 km^2). Diamonds indicate the times at which time averages (3-point means) in divergence were available.

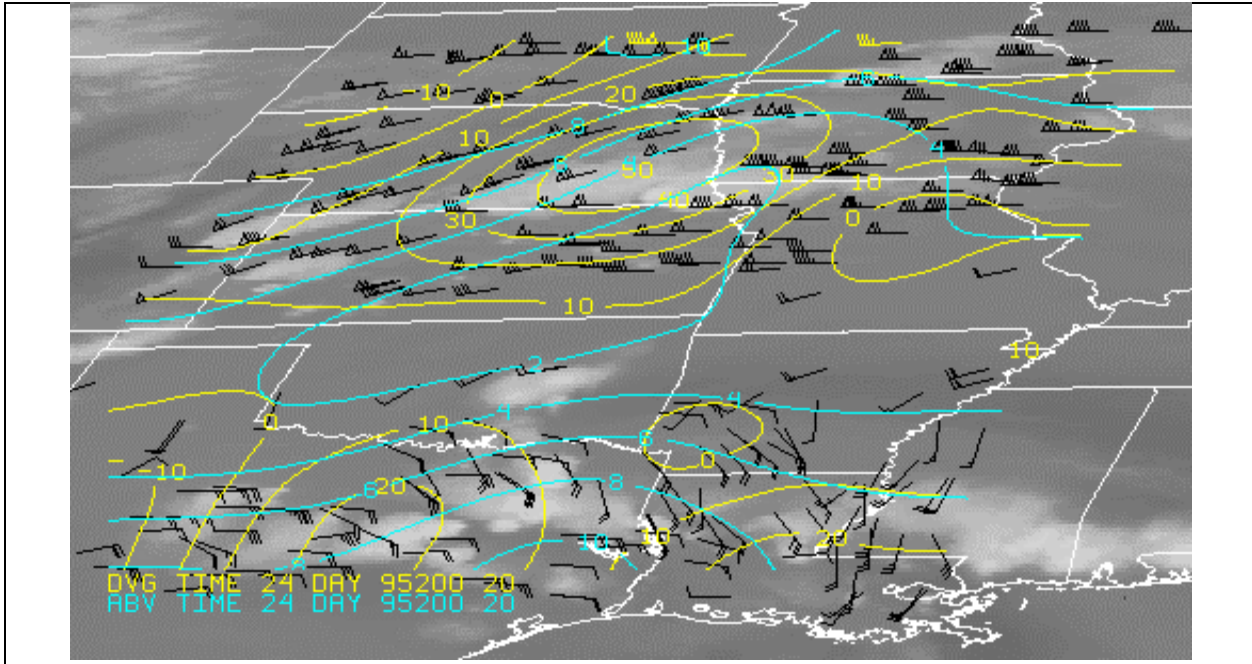


Figure 2a.

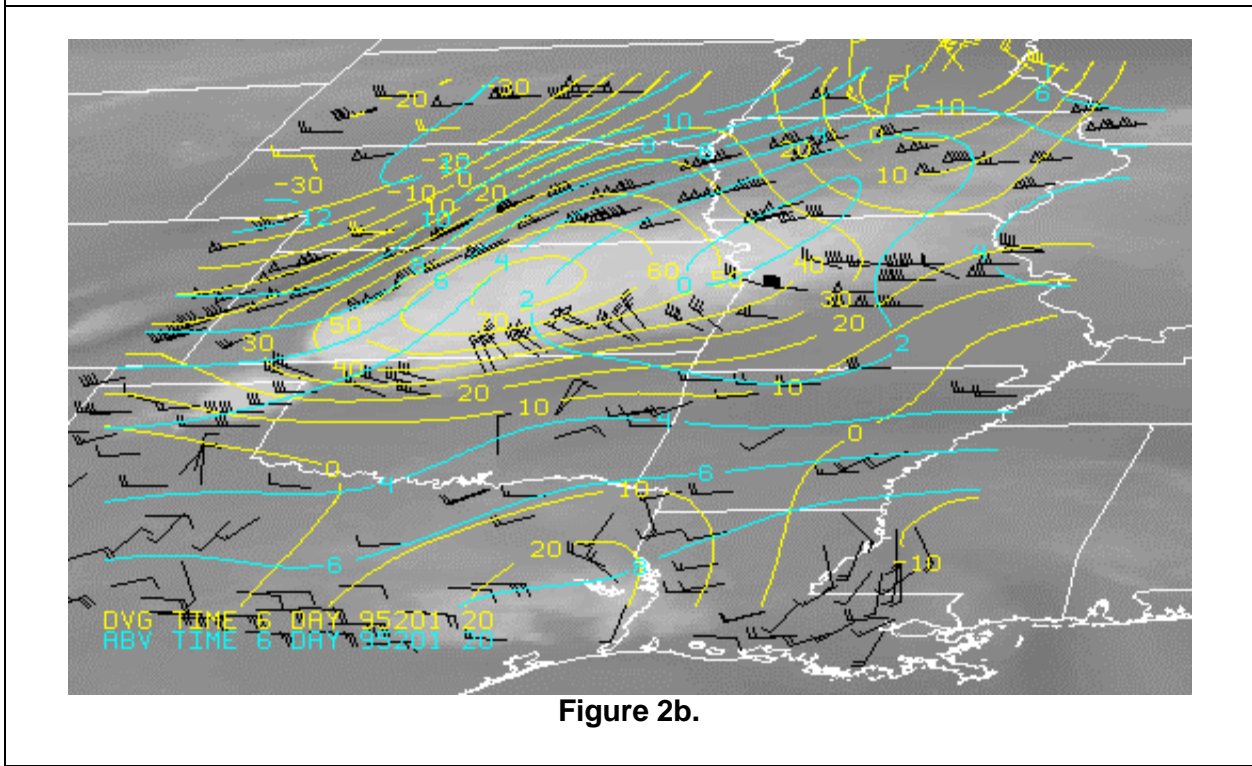


Figure 2b.

Figure 2. GOES-8 water vapour imagery, divergence (yellow, 10^{-5}s^{-1}), and absolute vorticity (red, 10^{-5}s^{-1}) at: a) 2300 UTC 19 July 1995, and b) 0445 UTC 20 July 1995.

Figure 3a.

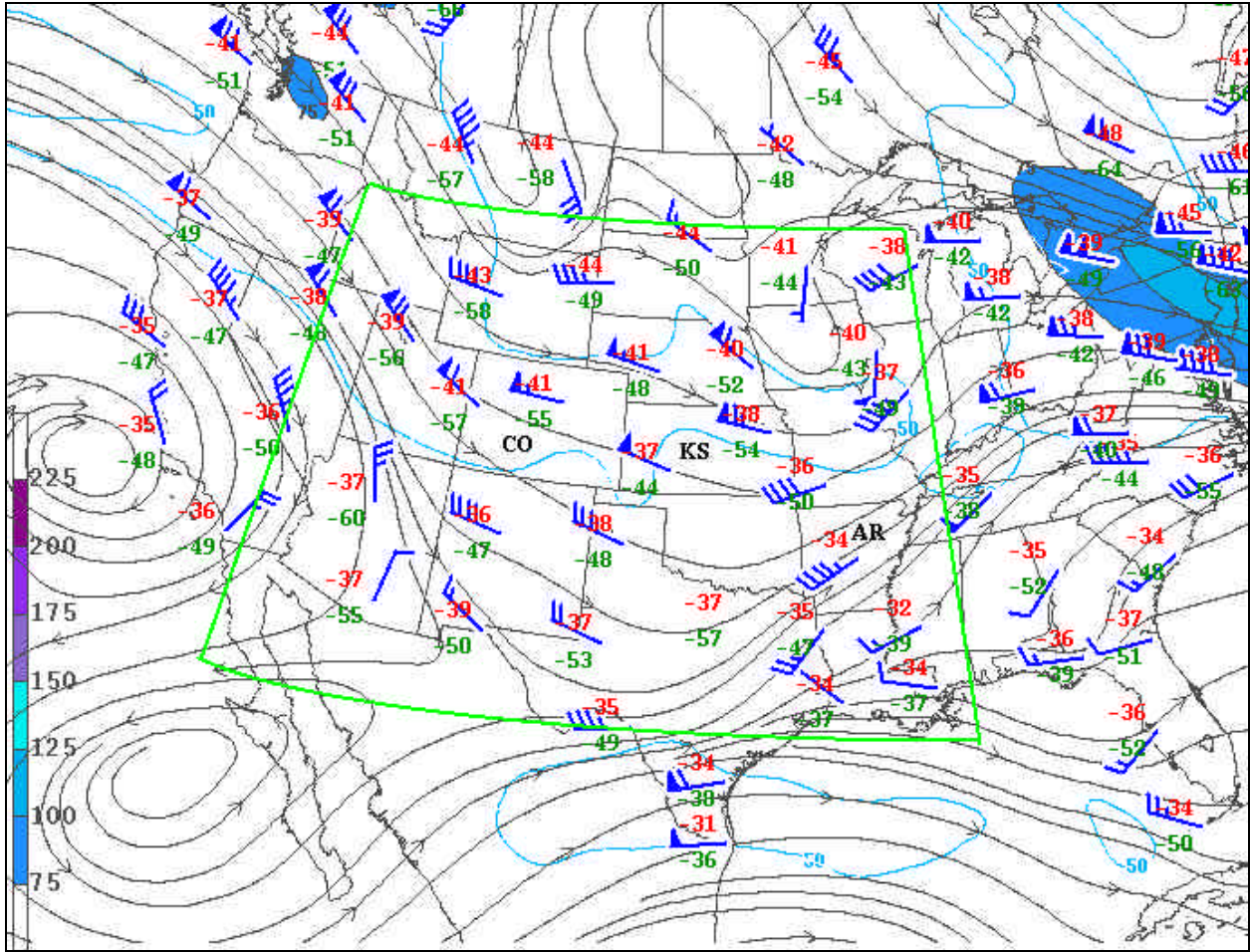


Figure 3b.

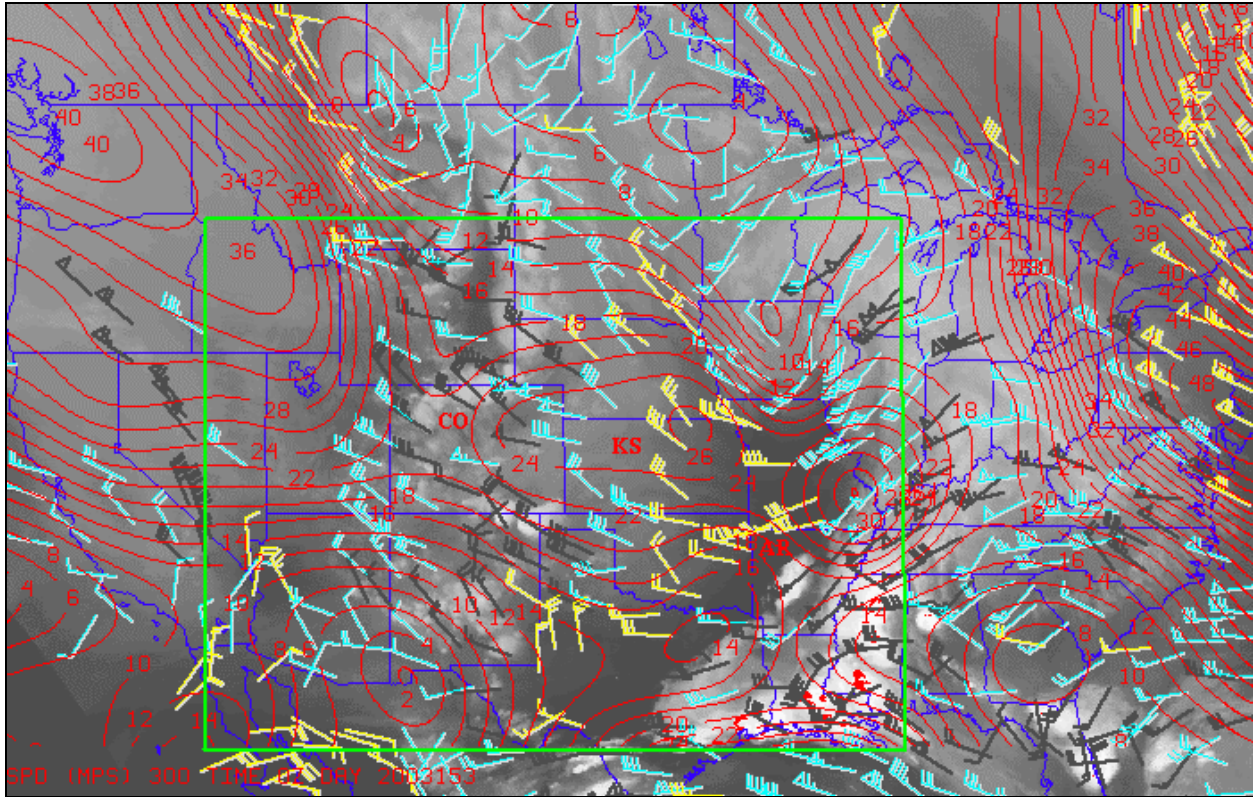


Figure 3. Upper air winds at 0000 UTC on 03 June 2003 from (a) synoptic weather balloons, and (b) satellite. The states of Colorado (CO), Kansas (KS), and Arkansas (AR) are noted. The area outlined in green is that shown in Figures 4-5. In (a), wind barbs (knots) are from observations at 300 hPa. Streamlines (grey) and isotachs (blue): 50, 75, and 100 kt (25, 32, and 50 ms^{-1}) are included. In (b), isotachs (red, knots) are from objectively analysed winds at 300 hPa (ms^{-1}), wind barbs (knots) are from the satellite-based winds (the average pressure of these wind vary, black: 100-250, cyan: 251-350, yellow: 351-500 hPa). Water vapour imagery is in the background.

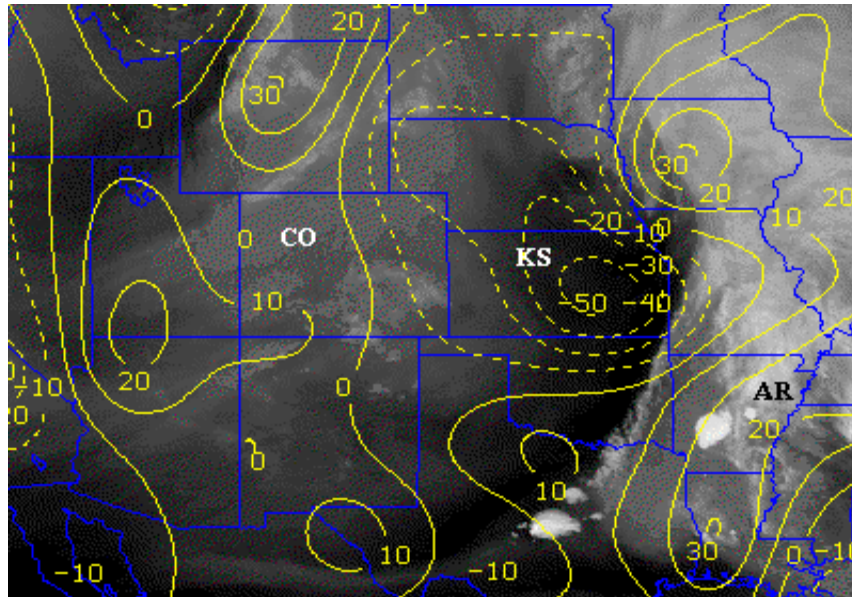


Figure 4a.

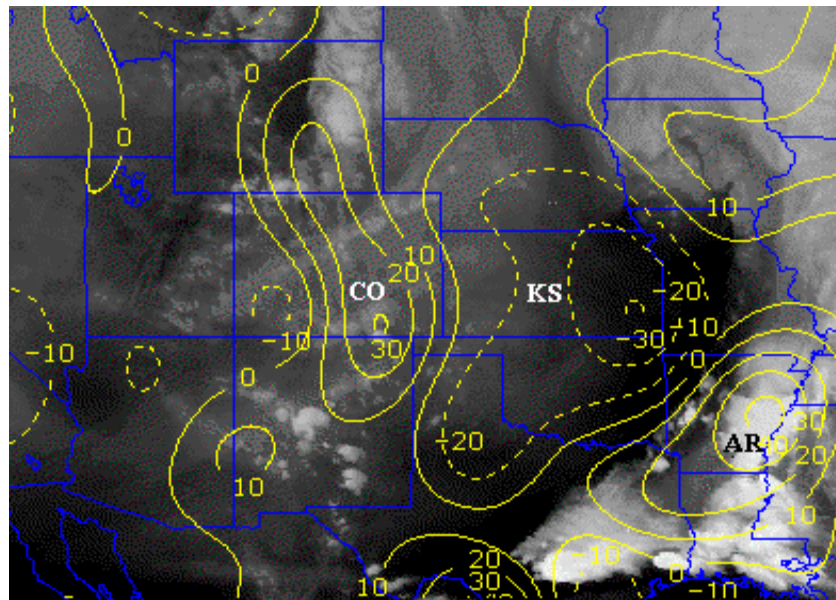


Figure 4b.

Figure 4. GOES-12 water vapour imagery and divergence at 300 hPa (10^{-5}s^{-1}) derived from satellite-winds on 02 June 2003 at a) 1745 UTC and b) 2145 UTC. Solid contours are positive (divergence) and dash contours are negative (convergence).

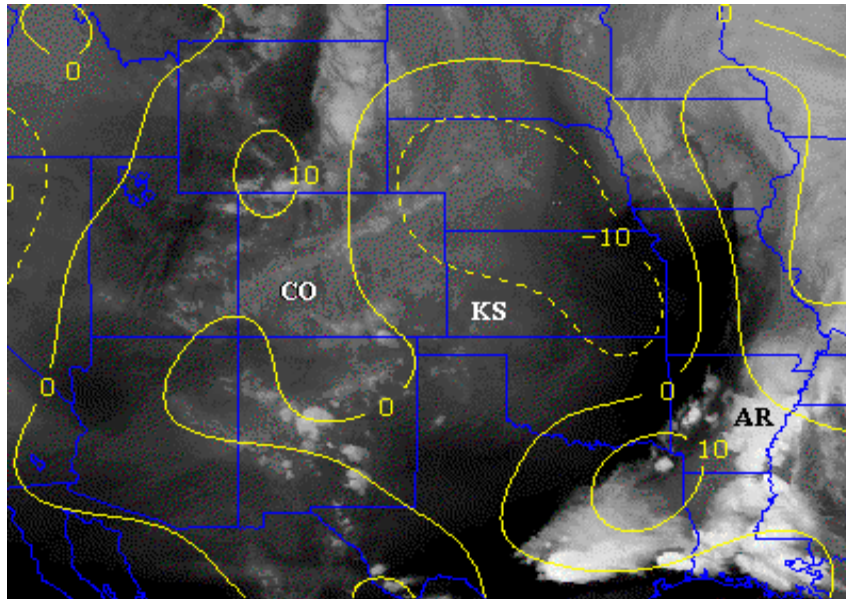


Figure 5a.

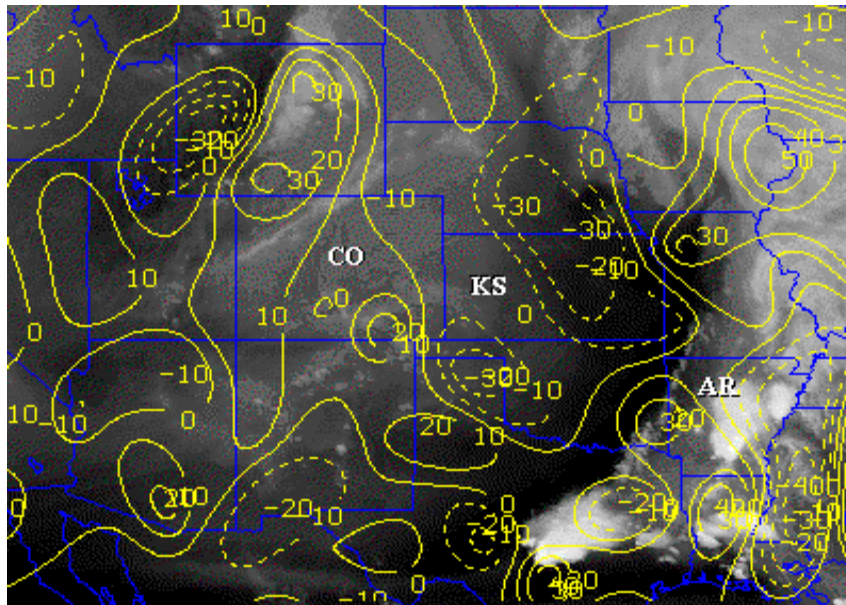


Figure 5b.

Figure 5. GOES-12 water vapour imagery and divergence at 300 hPa (10^{-5}s^{-1}) on 02 June 2003 at a) 2145 UTC, first guess (NOGAPS model), and b) 1945 UTC, RUC-2 mesoscale model analysis. Solid contours are positive (divergence) and dash contours are negative (convergence).

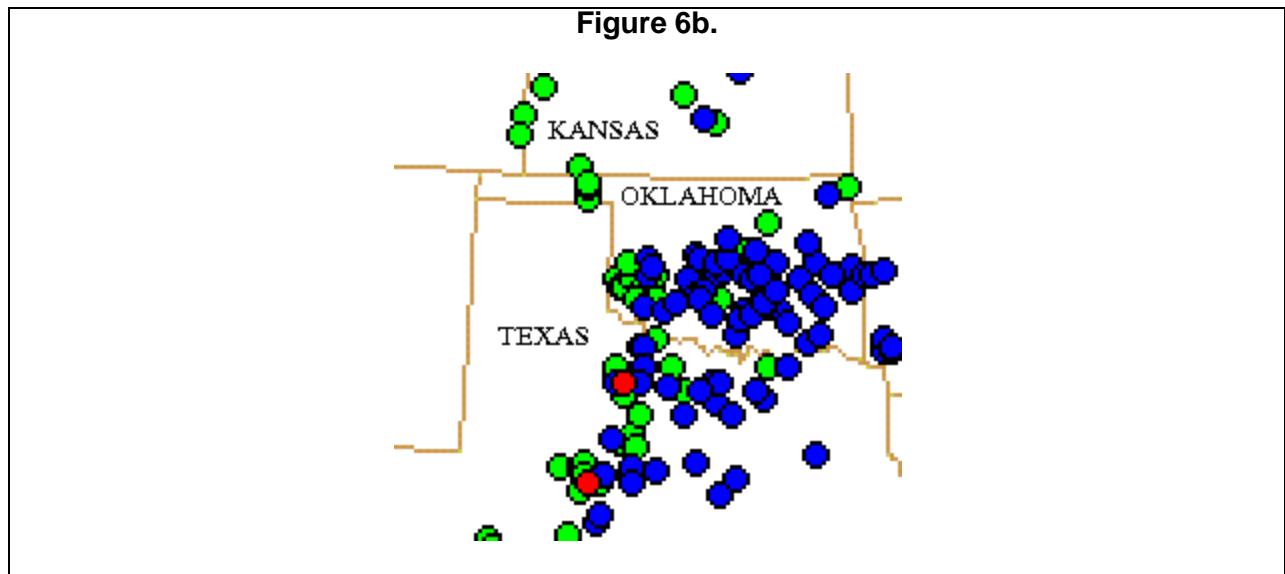


Figure 6. a) Surface weather map at 2300 UTC, 11 June 2003. Observations plotted are from the standard station model: wind flags (kts), temperature (upper left) and dew point (lower left) in degrees F, sea level pressure (upper right, last three digits of pressure in 10^{-1} hPa). Contours show sea level pressure (last two digits are labelled; for example, "04" indicates 1004 hPa). Fronts have solid barbs. Small barbs indicate outflow boundaries from rain-cooled air. Open barbs indicate a dryline (separating hot, dry air with a westerly wind component off the mountains from moist air with a southerly component from the Gulf of Mexico). Broken lines are dissipating fronts, b) Location of severe weather reports (courtesy of the NOAA/SPC) during the 24 hour period beginning at 1200 UTC on 11 June: wind damage (blue), large hail (green), and tornadoes (red).

Figure 7a.

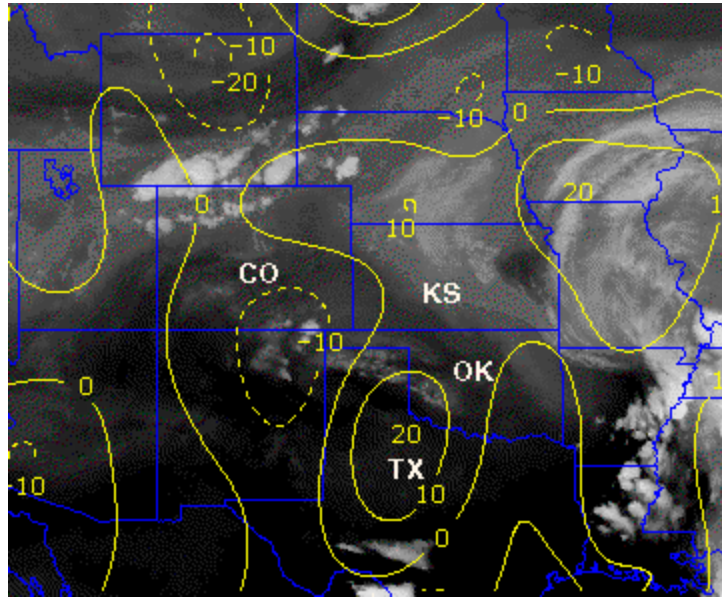


Figure 7b.

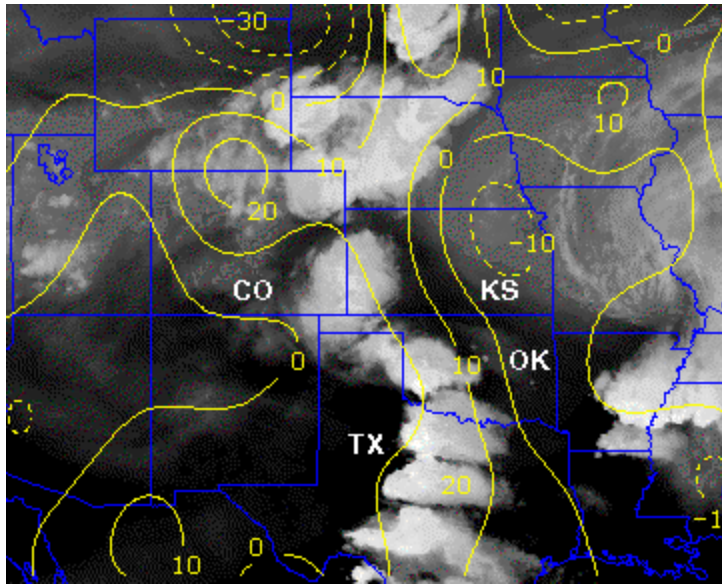


Figure 7. GOES-12 water vapour imagery and divergence at 300 hPa (10^{-5}s^{-1}) derived from satellite-winds, a) 11 June 2003 at 1945 UTC, b) 12 June 2003 at 0045 UTC. Solid contours are positive (divergence) and dash contours are negative (convergence).

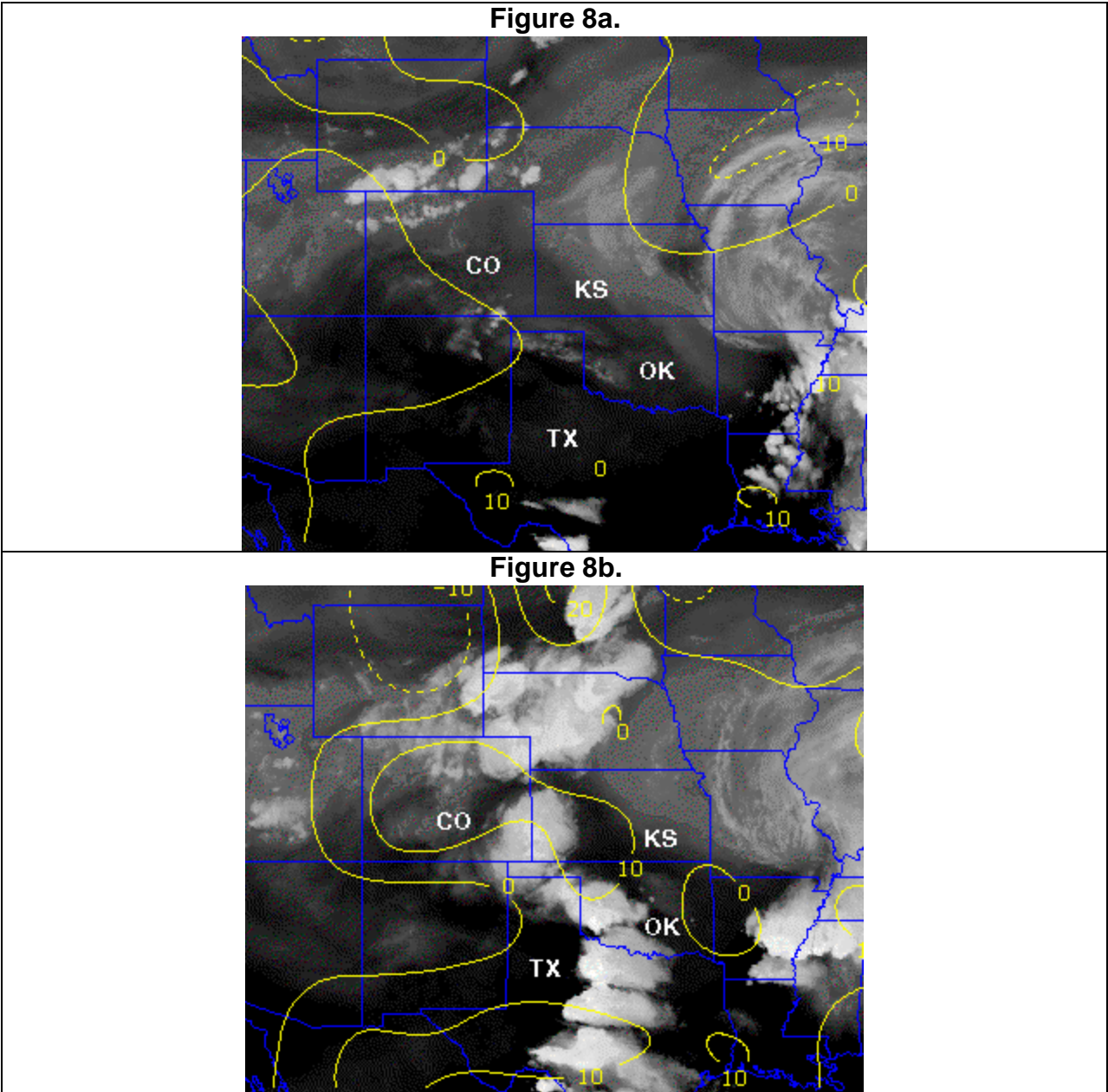


Figure 8. GOES-12 water vapour imagery and divergence at 300 hPa (10^{-5}s^{-1}) from first guess model (NOGAPS), a) 11 June 2003 at 1945 UTC, b) 12 June 2003 at 0045 UTC. Solid contours are positive (divergence) and dash contours are negative (convergence).

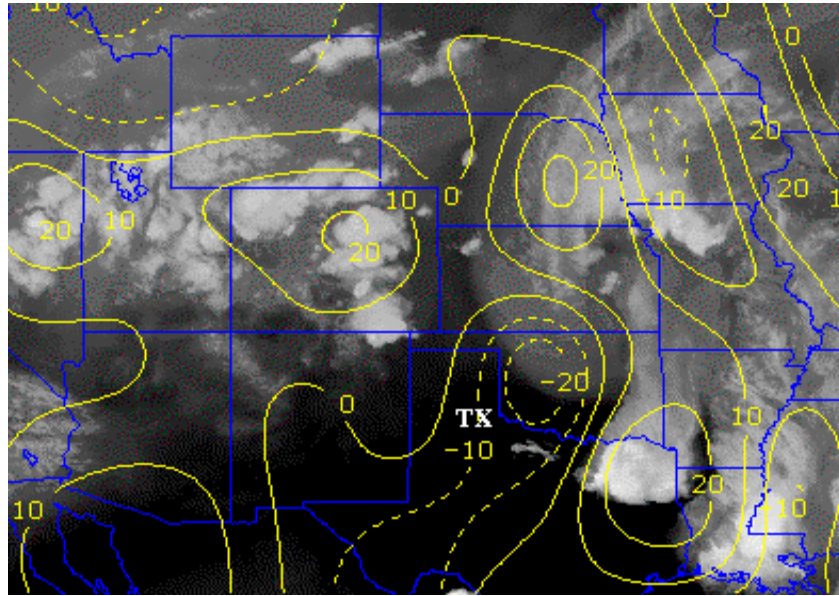


Figure 10a.

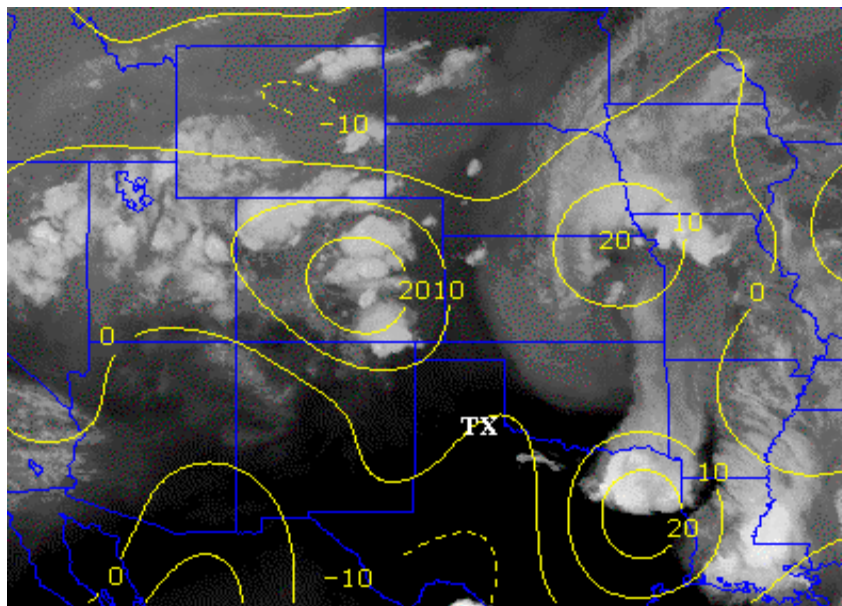


Figure 10b.

Figure 10. GOES-12 water vapour imagery and divergence at 300 hPa (10^{-5}s^{-1}) on 12 June 2003 at 2145 UTC, a) derived from satellite-winds, and b) first guess model (NOGAPS). Solid contours are positive (divergence) and dash contours are negative (convergence).